Peculiar Kinetics of the Complex Formation in the Iron(III)–Sulfate System

BALÁZS KORMÁNYOS, GÁBOR PEINTLER, ANDREA NAGY, ISTVÁN NAGYPÁL

Department of Physical Chemistry, University of Szeged, P.O. Box 105, H-6701 Szeged, Hungary

Received 16 April 2007; revised 23 August 2007; accepted 24 August 2007

DOI 10.1002/kin.20300
Published online in Wiley InterScience (www.interscience.wiley.com).

ABSTRACT: The results of comprehensive equilibrium and kinetic studies of the iron(III)–sulfate system in aqueous solutions at $I = 1.0$ M ($NaClO_4$), in the concentration ranges of $T_{Fe^{III}} = 0.15$–0.3 mM, $T_{SO_4^{2-}} = 3$–300 mM, and at pH 0.7–2.5 are presented. The iron(III)–containing species detected are $FeOH^{2+}$ (=FeH_{-1}), $(FeOH)_2^{4+}$ (=Fe_2H_{-2}), $FeSO_4^+$, and $Fe(SO_4)_2^-$ with formation constants of $\log \beta_{FeH_{-1}} = -2.84$, $\log \beta_{Fe_2H_{-2}} = -2.88$, $\log \beta_{FeSO_4^+} = 2.32$, and $\log \beta_{Fe(SO_4)_2^-} = 3.83$. The formation rate constants of the stepwise formation of the sulfate complexes are $k_{1a} = 4.4 \times 10^3\ M^{-1}\ s^{-1}$ for the $Fe^{3+} + SO_4^{2-} \underset{k_2}{\overset{k_{1a}}{\rightleftharpoons}} FeSO_4^+$ step and $k_2 = 1.1 \times 10^3\ M^{-1}\ s^{-1}$ for the $FeSO_4^+ + SO_4^{2-} \rightleftharpoons Fe(SO_4)_2^-$ step. The mono-sulfate complex is also formed in the $Fe(OH)^{2+} + SO_4^{2-} \xrightarrow{k_{1b}} FeSO_4^+$ reaction with the $k_{1b} = 2.7 \times 10^5\ M^{-1}\ s^{-1}$ rate constant. The most surprising result is, however, that the $2\ FeSO_4^+ \rightleftharpoons Fe^{3+} + Fe(SO_4)_2^-$ equilibrium is established well before the system as a whole reaches its equilibrium state, and the main path of the formation of $Fe(SO_4)_2^-$ is the above fast (on the stopped flow scale) equilibrium process. The use and advantages of our recently elaborated programs for the evaluation of equilibrium and kinetic experiments are briefly outlined. © 2008 Wiley Periodicals, Inc. Int J Chem Kinet 40: 114–124, 2008

INTRODUCTION

The formation of iron(III)–sulfate complexes has been studied by several researchers. Whiteker and Davidson [1] found spectrophotometrically that both $FeSO_4^+$ and $Fe(SO_4)_2^-$ species are formed at pH 0. Lister and Rivington [2] stated that $FeHSO_4^{2+}$ and $Fe(SO_4)(HSO_4)$ species also exist in the same pH range. Nikolajeva and Cvelodub [3] determined the temperature dependence of the formation constant of $FeSO_4^+$. Davis and Smith [4] determined the formation constants of $FeSO_4^+$ and $FeHSO_4^{2+}$ by supposing that $Fe(SO_4)_2^-$ is not formed in Fe^{3+} excess. Sapieszko et al. [5] proposed that the $NaSO_4^-$ ion pair formation is responsible for the experienced discrepancies concerning to the composition of the species. Khoe and Robins [6] found by pH-metric investigation that $Fe(OH)SO_4$ and $Fe_3(OH)_5SO_4^{2+}$ species exist in the $1.7 < pH < 3.3$ range. They have not found any protonated iron(III)–sulfate complex. Stipp [7] stated that the uncertainties of the speciation in the iron(III)–sulfate–water system make impossible the characterization of the processes in mine water.

The equilibrium was also studied theoretically. Brown and Sylva [8] estimated the formation constant by a unified theory, whereas Feng and Waki [9]

Correspondence to: Balázs Kormányos; e-mail: nagypal@chem.u-szeged.hu.

Contract grant sponsor: National Science Foundation of Hungary (OTKA).
Contract grant numbers: T 029838 and T 017257.

investigated the influence of the ionic medium on the formation constant of $FeSO_4^+$.

The kinetic of the complexation was also studied intensively by the pressure surge relaxation method [10], continuous-flow method with spectrometry [4], temperature jump investigation [11], stopped-flow method [12], and combined stopped-flow temperature jump techniques [5]. Most of these works were carried out in large iron(III) excess to avoid the formation of $Fe(SO_4)_2(OH)_x^{(x+1)-}$ $(x = -1, \ldots, 2)$ species, so a comprehensive investigation of the kinetics is still missing.

The aim of our present work is to set up a consistent equilibrium and kinetic model of the complex formation in the same pH range and to resolve the contradictions found in the previous literature. This goal required a comprehensive experimental reinvestigation and the use of recently developed evaluation methods [13–17] for handling large absorbance matrices provided by today's instruments.

MATERIALS AND METHODS

All the materials used were the commercially highest grade available. Deoxygenized MilliQ quality water was used in all experiments. The Na_2SO_4 stock solutions were prepared by dissolving anhydrous Na_2SO_4 (Reanal, Budapest, Hungary). The H_2SO_4 and $HClO_4$ stock solutions were diluted from conc. H_2SO_4 (Carlo Erba, Rodano, Italy) and conc. $HClO_4$ (Merck, Darmstadt, Germany), respectively. The iron(III) stock solution was prepared by dissolving $Fe(ClO_4)_3 \cdot xH_2O$ (Aldrich, Milwaukee, WI, USA) in the appropriate volume of $HClO_4$ stock solution. The pH of the solutions was adjusted by either H_2SO_4 or $HClO_4$ stock solutions, whichever was appropriate. The ionic strength was set to 1.0 M during all measurements, and it was adjusted with $NaClO_4$ (Merck) stock solutions.

All the samples were prepared in the same volumetric flask by diluting the appropriate amount of the stock solutions. Before the measurements were carried out, they had been thermostatted for 4 days in plastic vessels to reach the hydrolytic equilibrium. The temperature was $(25.0 \pm 0.2)^\circ C$ during the preparation and the measurements.

Standard acid–base titration was used to determine the concentrations in the H_2SO_4 and $HClO_4$ solutions, and complexometric titration with EDTA was used for the Fe^{III} concentrations. The contents of the Na_2SO_4 and $NaClO_4$ solutions were determined by standard gravimetric procedures.

The spectra in equilibrium state were recorded by a Zeiss Specord S10 UV–vis spectrophotometer. The kinetic traces were followed by a Hi-Tech SF-61 stopped-flow instrument with M300 spectrophotometer.

Equilibrium Study

Based on some preliminary experiments, two series of measurements were planned and carried out. The first one was recording the spectra of 45 different samples (see sets 1–5 in Table I and Fig. S1 in the Supplementary Material) to determine the formation constants of the hydrolytic equilibrium. This series was planned in the same way as it was reported earlier [17].

The second series included the recording of spectra of 75 different samples (see sets 6–12 in Table I and Fig. S2) to determine the compositions and formation constants of the sulfate-containing complexes. The widest experimentally achievable ranges of T_{H^+} and $T_{SO_4^{2-}}$ were applied for planning this series.

Kinetic Study

The samples were planned after the evaluation of the equilibrium measurements. Eighteen kinetic runs in three series were necessary to cover the whole measurable concentration ranges (see Table II). In one series, the total concentration of the sulfate changed whereas the pH was approximately constant. The kinetic traces were recorded at 274 and 304 nm; they included 1024 data pairs, and every shot was repeated 10 times. Two main considerations were applied when the initial concentrations of the solutions to be mixed were optimized:

Table I Total Concentrations in the Sets of the Equilibrium Measurements

Sets	$T_{Fe^{III}}$ (mM)	T_{H^+} (mM)	$T_{SO_4^{2-}}$ (mM)	Runs
		Fe^{III} hydrolysis		
1	0.1574	1, 2, 3, 5, 10, 20, 30, 50, 100	–	9
2–5	0.2361, 0.3148 0.4722, 0.6296	Set 1	–	9, 9, 9, 9
		Fe^{III}–SO_4^{2-} equilibrium		
6	0.1618	20	0, 3, 6, 10, 15, 22, 35, 50, 80, 120, 200, 340	12
7–8	Set 6	60, 200	Set 6	12, 12
9–11	0.3236	Sets 6–8	Set 6	12, 12, 12
12		20 60 200	10 30 100	3

Table II Total Concentrations of the Kinetic Measurements in the Solutions Before (F and S) and After (FS) mixing

		F	S		FS	
		$T_{Fe^{III}} = 0.6$ $T_{SO_4^{2-}} = 0.0$	$T_{Fe^{III}} = 0.0$		$T_{Fe^{III}} = 0.3$	
No.	pH	T_{H^+}	$T_{SO_4^{2-}}$	T_{H^+}	$T_{SO_4^{2-}}$	T_{H^+}
1	0.70	198	6	202	3	
2	0.72	193	20	207	10	
3	0.73	185	40	215	20	
4	0.78	165	100	235	50	200
5	0.87	134	200	266	100	
6	0.97	108	300	292	150	
7	1.23	58.6	6	61.4	3	
8	1.26	55.5	20	64.5	10	
9	1.29	51.4	40	68.6	20	
10	1.39	41.2	100	78.8	50	60
11	1.53	29.6	200	90.4	100	
12	1.65	22.5	300	97.5	150	
13	1.62	24.2	6	25.8	3	
14	1.65	22.5	20	27.5	10	
15	1.69	20.4	40	29.6	20	
16	1.81	15.6	100	34.4	50	25
17	1.96	10.9	200	39.1	100	
18	2.08	8.3	300	41.7	150	

The data are given in mM.

- The pH had to be the same before and after mixing to avoid the small effects of the relatively slow hydrolytic steps incidentally occurring in iron(III) solutions [18].
- The absorbance effects of $(FeOH)_2^{4+}$ should be negligible. This requirement limited the applicable pH range ($pH_{max} \approx 2$), so the $[(FeOH)_2^{4+}]_0/T_{Fe^{III}}$ ratio was less than 0.5% in each measured solution. It also resulted that the highest contribution of $(FeOH)_2^{4+}$ to the measured absorbances was 0.005 and 0.002 absorbance unit (AU) at 274 and 304 nm, respectively.

RESULTS

Equilibrium

The data measured in the 273–450-nm wavelength range were extracted and used for the further calculations. All absorbances in this range were lower than 1.1 AU. Larger absorbances measured at lower wavelengths were outside the most precise range of the spectrophotometer.

At first, model-free calculations were carried out on the absorbances by matrix rank analysis [15] and by the simplex method of linear programming [16]. These algorithms are able to determine the number of linearly independent absorbing species (NIAS), but they are unable to give the composition of those species. Both methods led to the following conclusions:

- NIAS = 3, when the spectra characterizing only the hydrolytic equilibrium were taken into account (sets 1–5 in Table I).
- NIAS = 5, when the spectra characterizing the sulfate complex formation were used (sets 6–12 in Table I).
- NIAS = 5, when the calculations were carried out with the whole absorbance matrix (sets 1–12 in Table I). Figure 1 illustrates this result. Although the supposed number of the absorbing species was less than 5, large and systematic deviations could be seen, comparing the residual absorbances to the experimental uncertainty, which had been ~0.002 AU. The extent of this deviation

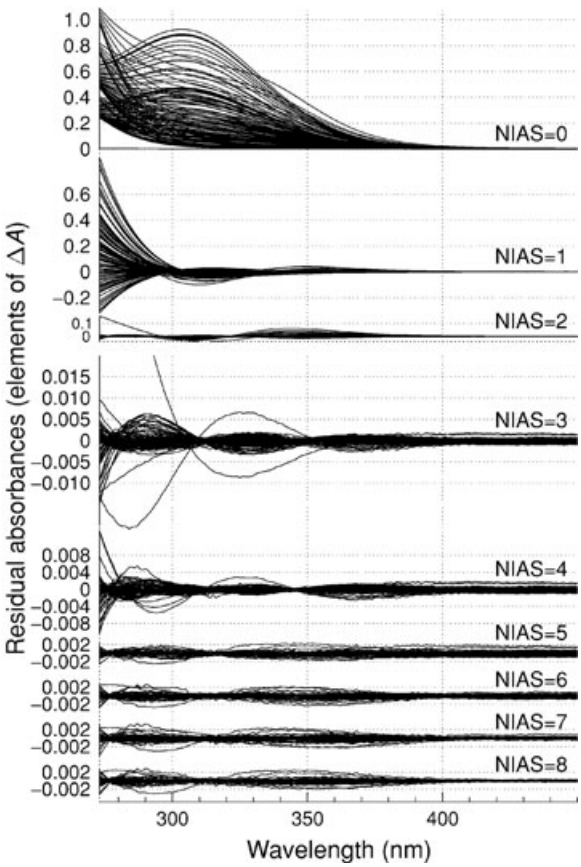

Figure 1 Result of the absorbance matrix resolution ($\boldsymbol{A} = \boldsymbol{\varepsilon} \times \boldsymbol{c} + \boldsymbol{\Delta A}$) with the $\mathcal{M}^3$ program [16]. A group of the curves shows the unexplained absorbance errors (i.e., the elements of $\boldsymbol{\Delta A}$) at a given number of absorbing species (NIAS).

Table III Composition of the Species Considered in the Equilibrium Calculations

$Fe_xH_y^{(3x+y)+}$	x	**1**	**0**	**1**	**2**	1	2	2	3	3	4
	y	**0**	**1**	**−1**	**−2**	−2	−1	−3	−3	−4	−4
$Fe_xH_y(SO_4)_z^{(3x+y-2z)+}$	x	**0**	**0**	**1**	**1**	1	1	1	1	1	1
	y	**0**	**1**	**0**	**0**	1	1	−1	0	0	−2
	z	**1**	**1**	**1**	**2**	1	2	1	3	4	1

Boldfaced numbers indicate the species included in the final model.

was decreasing with larger value for NIAS. After the inclusion of the fifth species, the shape of the residual absorbance curves did not show any systematic change outside the experimental error. Furthermore, the inclusion of the species beyond the fifth absorbing species did not decrease the residual absorbance significantly or systematically.

These results have proven that five absorbing species are important in the investigated concentration ranges. Three of them should be derived from the hydrolysis of iron(III)–hexaaqua complex and two of them are iron(III)–sulfate complexes (with unknown composition yet).

The composition and the formation constants of the existing species were determined by PSEQUAD [13] using nonlinear parameter estimation. All species were taken into consideration that were reported in the previous literature as existing ones in our investigated concentration range (see Table III). Each possible equilibrium model including iron(III), two hydrolytic species, HSO_4^-, and two or three sulfate complexes were tried. Finally, the following five formation constants have proven to be necessary to describe the experiments:

$$\beta_{1-10} = \frac{[FeOH^{2+}][H^+]}{[Fe^{3+}]}, \quad \lg \beta_{1-10} = -2.843 \pm 0.012 \tag{E1}$$

$$\beta_{2-20} = \frac{\left[(FeOH)_2^{4+}\right][H^+]^2}{[Fe^{3+}]^2}, \quad \lg \beta_{2-20} = -2.880 \pm 0.080 \tag{E2}$$

$$\beta_{011} = \frac{[HSO_4^-]}{[H^+]\left[SO_4^{2-}\right]}, \quad \lg \beta_{011} = 1.174 \pm 0.003 \tag{E3}$$

$$\beta_{101} = \frac{[FeSO_4^+]}{[Fe^{3+}]\left[SO_4^{2-}\right]}, \quad \lg \beta_{101} = 2.324 \pm 0.021 \tag{E4}$$

$$\beta_{102} = \frac{[Fe(SO_4)_2^-]}{[Fe^{3+}]\left[SO_4^{2-}\right]^2}, \quad \lg \beta_{102} = 3.834 \pm 0.031 \tag{E5}$$

For this model, the average deviation between the experimental and calculated data (σ) was 0.0020 AU, and there was no systematic change in this value as a function of total concentrations. Other models led to

Table IV Formation Constants for Species in Iron(III) and Sulfate Containing Aqueous Solutions at 25°C

$\lg \beta_{1-10}$	$\lg \beta_{2-20}$	$\lg \beta_{011}$	$\lg \beta_{101}$	$\lg \beta_{102}$	Medium	Ref.
–	–	–	2.03	3.00	~1 M $NaClO_4$	[1]
–2.83	–	1.22	–	–	1.0 M $NaClO_4$	[5]
–2.93	–3.22	1.14	1.92	–	2.7 M $NaClO_4$	[5]
–3.01	–3.09	1.10	0.41	–	1.0 M $NaNO_3$	[6]
–	–	–	2.58	–	0.4 M $NaClO_4$	[10]
–2.52	–	1.76	2.78	5.03	~0.075 M $NaClO_4$	[11]
–2.73	–	1.36	2.31	–	0.5 M $NaClO_4$	[12]
–2.81	–	1.17	2.12	–	1.2 M $NaClO_4$	[12]
–2.85	–	1.08	2.04	–	2.0 M $NaClO_4$	[12]
–2.72	–	1.36	2.31	–	0.5 M $NaClO_4$	[7]
–2.77	–2.81	–	–	–	0.5 M $NaClO_4$	[17]
–2.72	–2.86	–	–	–	1.0 M $NaClO_4$	[18]
–2.84	–2.88	1.17	2.32	3.83	1.0 M $NaClO_4$	This work

βs are defined in Eqs. (E1)–(E5).

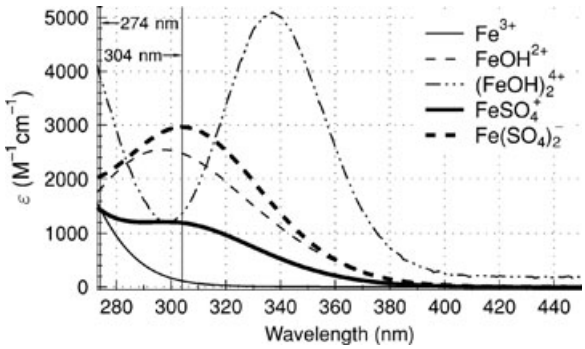

Figure 2 Calculated molar absorbance spectra of the iron(III)-containing species. The vertical lines indicate the wavelengths used for kinetic measurements.

either much higher value for σ, negligible concentrations or total correlations between the fitted parameters. The concentration distributions of the Fe^{III}-containing species are shown in Fig. S3 as a function of the total sulfate concentration.

Table IV summarizes the formation constants reported in the previous literature. Although some discrepancies can be found, our β_{1-10} and β_{2-20} values are in good agreement with the most recently reported values [17, 18]. The effect of β_{011} will be analyzed in the discussion. Our value for β_{101} is almost the average of the previously determined values. β_{102} has only two different literature values, and these ones differ from each other by 2 orders of magnitude so the comparison is not possible.

The calculation gave the molar absorbances, as well, as seen in Fig. 2. These curves suggested two wavelengths for the kinetic study: The largest differences between the molar absorbances of Fe^{3+}, $FeSO_4^+$, and $Fe(SO_4)_2^-$ are at 304 nm, and the most independent experimental information for $Fe(SO_4)_2^-$ can be collected at 274 nm since Fe^{3+} and $FeSO_4^+$ have the same molar absorbance.

Kinetics

The median curves of the 10 shots from each sample were chosen for the evaluation. As the first step, exponential curve-fitting techniques were applied. Each curve was found to be pseudo-first order as illustrated in Fig. S4.

Second, the data at 304 nm were plotted against the data measured at 274 nm for all traces and the result was always a straight line. It is easy to realize that this parametric plot gives a straight line only if both absorbance vs. time curves can be characterized by the same pseudo-first-order rate constant, that is, independent kinetic information cannot be extracted

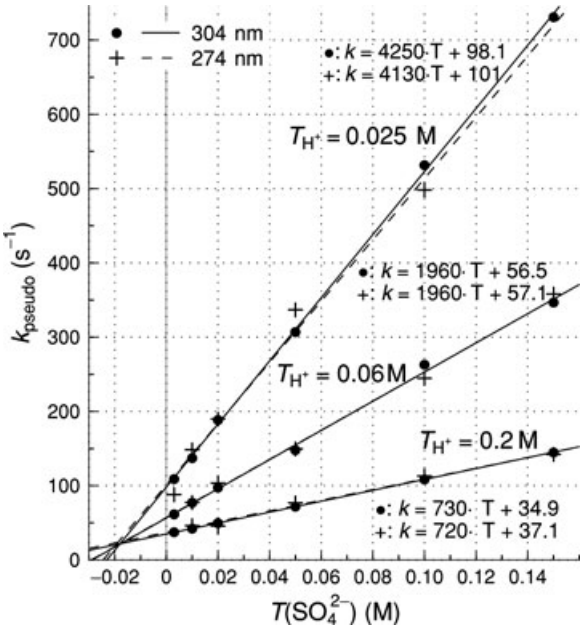

Figure 3 Pseudo-first-order rate constants as a function of total sulfate concentration. The symbols are the pseudo-first-order rate constants fitted curve by curve. The legends give the parameters of the fitted straight lines. The interpretation of this figure is given in the text.

at different wavelengths. The worst linear relation is illustrated in Fig. S5. This figure also presents that the experimental uncertainty is ∼0.003 AU.

The calculated pseudo-first-order rate constants were plotted against the total sulfate concentration as shown in Fig. 3. At a constant T_{H^+} value, the relation is linear independently on the wavelength used and both the slope and the intercept become higher with increasing pH. This simple relation—with the assumption that the $FeSO_4^+$ formation and dissociation determine the rate of the reaction—makes possible to calculate β_{101} from the kinetic data. However, the calculated value is very far from the value determined by the equilibrium measurements as we discuss it later. Another unexpected fact is that the three straight lines have a common cross-point (at $T_{SO_4^{2-}} = -0.018 \pm 0.002$ M and $k_{pseudo} = 22 \pm 4$ s^{-1}). These findings indicate an unusual kinetics.

ZiTa [14], a multipurpose kinetic program package, was used to find the kinetics of the complexation. The program is suitable for simultaneous evaluation of any number of experimental curves to be described by the same kinetic model and parameter set. Almost 2000 configurable options make possible to handle any kind of kinetic model and any transformation between the primary measured signals and the concentrations. ZiTa is also able to consider any relation or constraint between the parameters.

Table V Finally Proposed Steps for the Formation of the Iron(III)–Sulfate Complexes

No.	Reaction Step	k_b (s^{-1})	k_f (M^{-1} s^{-1})	$k_f^i =$
(R1)	$SO_4^{2-}+H^+ \underset{k_b}{\overset{k_f}{\rightleftharpoons}} HSO_4^-$	$\geq 10^5$	$\geq 1.5\times10^6$	$k_b^1\cdot\beta_{011}$
(R2)	$FeOH^{2+}+H^+ \underset{k_b}{\overset{k_f}{\rightleftharpoons}} Fe^{3+}$	$\geq 10^5$	$\geq 7.0\times10^7$	k_b^2/β_{1-10}
(R3)	$Fe^{3+}+SO_4^{2-} \underset{k_b}{\overset{k_f}{\rightleftharpoons}} FeSO_4^+$	20.8 ± 0.3	$(4.4\pm0.2)\times10^3$	$k_b^3\cdot\beta_{101}$
(R4)	$FeOH^{2+}+SO_4^{2-} \underset{k_b}{\overset{k_f}{\rightleftharpoons}} Fe(OH)SO_4$	$\frac{1.81\pm0.02}{k_b^5/k_f^5}$	$(2.7\pm0.1)\times10^5$	$k_b^4\cdot\frac{k_b^5}{k_f^5}\cdot\frac{\beta_{101}}{\beta_{1-10}}$
(R5)	$Fe(OH)SO_4+H^+ \underset{k_b}{\overset{k_f}{\rightleftharpoons}} FeSO_4^+$	$\geq 10^4$	$\geq 10^4\cdot k_b^5$	
(R6)	$FeSO_4^++SO_4^{2-} \underset{k_b}{\overset{k_f}{\rightleftharpoons}} Fe(SO_4)_2^-$	34.2 ± 0.9	$(1.1\pm0.1)\times10^3$	$k_b^6\cdot\frac{\beta_{102}}{\beta_{101}}$
(R7)	$Fe^{3+}+Fe(SO_4)_2^- \underset{k_b}{\overset{k_f}{\rightleftharpoons}} 2FeSO_4^+$	$\geq 2\times10^7\ M^{-1}$	$\geq 1.3\times10^8$	$k_b^7\cdot\frac{\beta_{101}^2}{\beta_{102}}$
(R3b)	$FeOH^{2+}+HSO_4^- \underset{k_b}{\overset{k_f}{\rightleftharpoons}} FeSO_4^+$	$\equiv k_b^3$	$(2.1\pm0.1)\times10^5$	$k_b^{3b}\cdot\frac{\beta_{101}}{\beta_{1-10}\cdot\beta_{011}}$
(R7b)	$FeOH^{2+}+Fe(SO_4)_2^- \underset{k_b}{\overset{k_f}{\rightleftharpoons}} Fe(OH)SO_4+FeSO_4^+$	$\geq 10^{10}\ M^{-1}$	$\geq 4.5\times10^{13}\cdot\frac{k_b^5}{k_f^5}$	$k_b^{7b}\cdot\frac{k_b^5}{k_f^5}\cdot\frac{\beta_{101}^2}{\beta_{102}\cdot\beta_{1-10}}$

For faster calculations, the experimental curves have been filtered to decrease the number of data. Fifty data pairs were chosen to describe the shape of the curves. Filtering resulted 1800 data pairs (18 kinetic traces, 2 wavelengths), and they were used together for the further calculations.

About 50 kinetic models were tried during the calculations. They included different combinations of 18 chemically acceptable equilibrium steps, such as the reactions of the species playing role in equilibrium and the reactions of possible intermediates such as $FeHSO_4^{2+}$, $FeH(SO_4)_2$, $Fe(OH)SO_4$, $Fe_2(SO_4)_2^{2+}$, and $Fe(SO_4)_3^{3-}$. Every calculation was carried out under the following conditions:

- The molar absorbance values of Fe^{3+}, $FeOH^{2+}$, $(FeOH)_2^{4+}$, $FeSO_4^+$, and $Fe(SO_4)_2^-$ had already been determined, and they were always fixed during the kinetic calculations. The molar absorbances of the possible intermediates were either fitted or omitted.
- The initial concentrations of the solutions to be mixed were calculated from the total concentrations and the formation constants.
- The formation constants defined in (E1)–(E5) were fixed in all calculations.
- Since the rate constants of an equilibrium step are not independent of each other, the backward rate constants (k_b-s) were always fitted. The forward rate constants (k_f-s) were calculated from k_b-s and the formation constants. The used formulae are given in the last column of Table V.
- It was already proven earlier [17] that the dead time conception is not applicable when all stopped-flow curves are evaluated simultaneously. Instead of the dead time, two other parameters are suitable: the filling time of the cuvette and the hypothetical starting time (t_0^h). The filling time can be measured by physical methods [17], so it was fixed to the determined 0.0035-s value. The hypothetical starting time is the time difference between the time of stopping the flow and the back-extrapolated value of the initial time of the homogeneous reaction. Its value cannot be determined independently, so the t_0^h values were fitted together with the rate constants.

The finally accepted mechanism and the rate constants calculated are given in Table V. The standard deviations of the backward rate constants were calculated by ZiTa [14]. The standard deviations of the forward rate constants were calculated from the deviations of k_b-s and from the deviations of the formation constants (β-s), taking the error propagation into account [19].

Steps (R1, R2) are fast preequilibria, only minimal values of their rate constants can be given.

Steps (R3, R4, R5) are responsible for the formation of $FeSO_4^+$.* (R3) is one of the rate-determining steps in the kinetics of complexation. Step (R4) explains the pH-dependence of the $FeSO_4^+$ formation through the fast (R2) preequilibrium process. (R5) must be very fast compared to (R4). In this way, the pH dependence of (R5) does not appear in the measurable reaction rate. $Fe(OH)SO_4$ has no significant contribution either to the absorbances or to the total iron(III) concentration. (R4) is the second rate-determining step.

Steps (R6, R7) are responsible for the formation of $Fe(SO_4)_2^-$. (R6) is slow; it is the third rate-determining

*(R3) and (R3b) cannot be distinguished from each other since these steps have mathematically equivalent rate equations. Either one of them or any combination of them gives the same result.

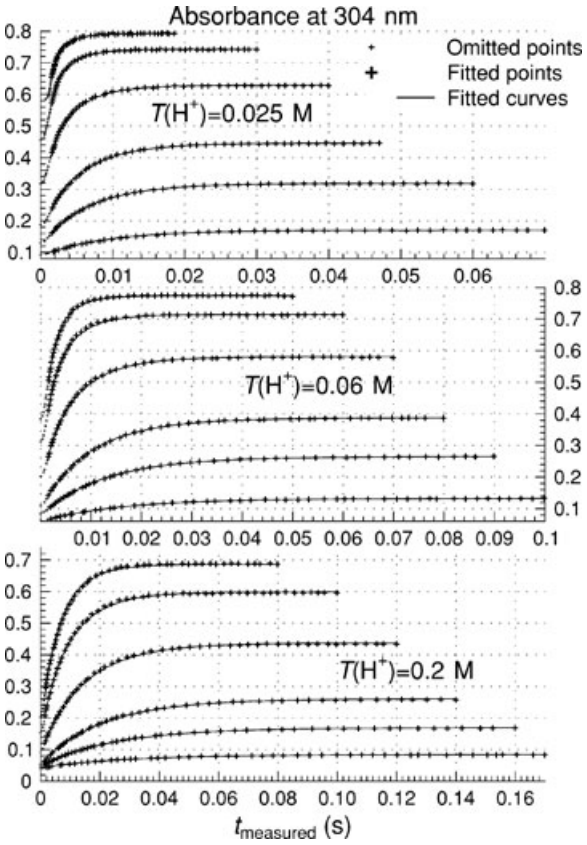

Figure 4 Experimental and calculated curves of the finally proposed mechanism. The initial concentrations are given in Table II. $\sigma = 0.0028$ AU for this calculation.

step whereas (R7) is fast, only minimal value for the rate constant can be given.† (R7) is a new step; it has not been reported earlier. Simulations have shown that (R6) plays significant role in the formation of $Fe(SO_4)_2^-$ only at the early stage of the reaction, whereas (R7) is important at the later stage.

Figure 4 presents the fitted experimental points (at 304 nm) and the calculated curves. This figure and every calculated statistical parameter have confirmed that our proposed mechanism describes the experiments very well. The importance of the individual steps can be explored by omitting them one by one. The first two rows of Table VI summarize the results focusing on the value of the average deviation. The first value shows that the proposed mechanism has a σ value corresponding to the experimental uncertainty. Figure 4 proves that this deviation is equally spread on the curves; no systematic change can be noticed along the time scale or changing total concentrations.

†Exclusive inclusion of (R7) or ((R7b), (R5)) gives entirely the same calculated curves; however, their rate equations are not equivalent mathematically. The fastness of these processes makes them indistinguishable, but the presence at least one of them is required.

Table VI The Average of the Absorbance Deviations (σ) of the Measured and Calculated Data for Different Time Models

Time model	σ (AU)				
$t_{\text{filling}} + t_0^h$	0.0028	0.0050	0.0078	0.0038	0.0056
t_{dead}	0.0051	0.0092	0.0164	0.0052	0.0090
Omitted step(s)	–	(R3)	(R4) (R5)	(R6)	(R7)

The interpretation of these values is given in the text.

Omission of any step from the proposed mechanism significantly increases the deviations above the experimental uncertainty. Moreover, these deviations appear systematically along the curves. The σ values in the table also show clearly that (R7) is more important for the formation of $Fe(SO_4)_2^-$ than the more plausible (R6).

Comparison of our kinetic data to the literature values is possible only for the formation of $FeSO_4^+$ since no data are available for $Fe(SO_4)_2^-$. Davis and Smith [4] found $k_f^3 = 6.3 \times 10^3\,M^{-1}\,s^{-1}$, but they did not notice pH dependence in the $T_{H^+} = 0.05$–0.3 M range. Wendt and Strehlow [10] reported only an approximate value ($\sim 10^3$) for k_f^3. Cavasino [11] found two values: $k_f^3 = 3.0 \times 10^3\,M^{-1}\,s^{-1}$ and $k_f^4 = 1.1 \times 10^5\,M^{-1}\,s^{-1}$. Baker and Smith [12] determined the $k_f^3 = 5.6 \times 10^3\,M^{-1}\,s^{-1}$ and $k_f^4 = 1.1 \times 10^5\,M^{-1}\,s^{-1}$. Taking the slightly different experimental conditions into account, the k_f^3 and k_f^4 values are in good agreement. Step $Fe^{3+} + HSO_4^- \rightleftharpoons FeHSO_4^{2+}$ was found by Cavasino [11], but according to our work its contribution cannot be detected.

DISCUSSION

Equilibrium

Against the proposals in the literature, protonated/deprotonated iron(III)-sulfate complexes could not be identified under our experimental conditions. The series of the measured spectra (given in Fig. S2), however, clearly show the pH independence of the complex formation as a function of $T_{SO_4^{2-}}$. Comparing the series of the spectra measured at $T_{H^+} = 0.2$, 0.06, and 0.02 M, it is obvious that the measured spectra belonging to the highest $T_{SO_4^{2-}}$ are practically identical independently of the value of T_{H^+}. It would be impossible if (de)protonation took place.

The equilibrium constant of the practically non-absorbing HSO_4^-/SO_4^{2-} was also calculated by PSEQUAD [13] making use of the principle of competitive photometry [20]. It is worth mentioning that if this constant is not calculated, but fixed at a value of

1.224 [21] instead of 1.174, then the formation of "new species," for example, $FeHSO_4^{2+}$ or $FeH(SO_4)_2$, may be concluded, showing how dangerous is to accept an auxiliary equilibrium constant from the literature when a complex equilibrium system is investigated.‡

Kinetics

Mechanism of the Complex Formation. In principle, it is not necessary to assume the presence of $Fe(OH)SO_4$ to interpret the pH-dependent reaction rate. Steps (R4) and (R5) may be replaced by the equilibrium processes

$$FeOH^{2+} + SO_4^{2-} \underset{k_b}{\overset{k_f}{\rightleftharpoons}} FeSO_4^{+}OH^{-} \qquad (R8)$$

$$H^{+} + OH^{-} \underset{k_b}{\overset{k_f}{\rightleftharpoons}} H_2O \qquad (R9)$$

With the replacement, the modified model calculated exactly the same curves as the proposed model but *only if* $k_f^9 > 10^{15}$ M^{-1} s^{-1}, which is obviously not realistic. That is why we suggest steps (R4) and (R5) instead of (R8) and (R9). With (R4) and (R5), no second-order rate constant above the diffusion controlled limit is necessary to characterize the system.

The most striking result of the evaluation is that the main path of the $Fe(SO_4)_2^-$ formation is the

$$Fe(SO_4)_2^- + Fe^{3+} \rightleftharpoons 2FeSO_4^+ \qquad (R7)$$

fast equilibrium. Its rate constants cannot be calculated, only a lower limit can be given (Table V). In other words, the reaction quotient of the above process corresponds to the equilibrium constant much before the system as a whole reaches its equilibrium state. To illustrate it, let us define the time-dependent reaction quotients by the

$$Q_1 = \frac{[FeSO_4^+]}{[Fe^{3+}][SO_4^{2-}]} \qquad \lim_{t\to\infty} Q_1 = K_1 \qquad (Q1)$$

$$Q_2 = \frac{[Fe(SO_4)_2^-]}{[FeSO_4^+][SO_4^{2-}]} \qquad \lim_{t\to\infty} Q_2 = K_2 \qquad (Q2)$$

$$Q_3 = \frac{[FeSO_4^+]^2}{[Fe(SO_4)_2^-][Fe^{3+}]} = \frac{Q_1}{Q_2} \qquad \lim_{t\to\infty} Q_3 = \frac{K_1}{K_2} \qquad (Q3)$$

equations. Figure 5 includes the calculated reaction quotients in a sample to show that the $Q_3 = K_3$ relation is valid in the whole measurable time range. A straightforward consequence of the fast equilibrium (R7) is that at higher $T_{SO_4^{2-}}$, the concentration of $FeSO_4^+$ as a function of time, goes through a maximum as it is seen in Fig. 6.

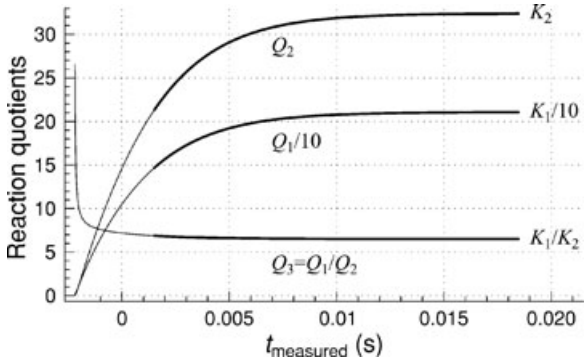

Figure 5 Calculated time-dependent reaction quotients in case of sample 13 (Table II). Q_i-s and K_i-s are defined by Eqs. (Q1), (Q2), and (Q3). Thicker lines denote the measurable time range.

It is generally accepted that the consecutive kinetic rate constants of a stepwise equilibrium system are sufficient to describe its kinetic behavior. Our results challenge this general belief. We put forward the

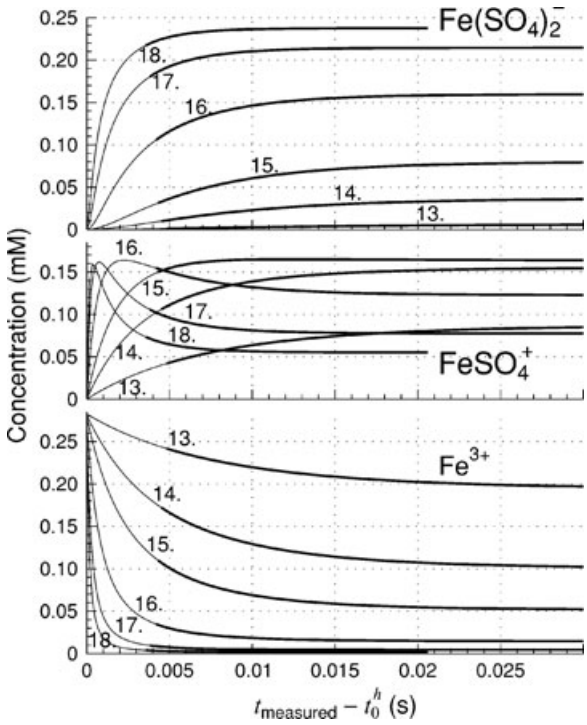

Figure 6 Calculated concentration vs. time curves for Fe^{3+} (bottom), $FeSO_4^+$ (center), and $Fe(SO_4)_2^-$ (top). The numbers of the curves correspond to the numbers in Table II. The thicker parts of the curves denote the time range in which experimental data are available.

‡The $\lg \beta_{011} = 1.224$ value is also the average of the data measured at 1.0 M ionic strength and collected from [21].

following considerations to interpret the peculiar kinetic behavior. In the cases of the Fe^{3+} and SO_4^{2-} ions, the formation of $FeSO_4^+$ requires the destruction of two symmetric hydrate spheres, and thus the process is relatively slow, in spite of the electrostatic attraction. The formal charge of $FeSO_4^+$ is +1, but it is in fact a dipole ion with partial positive and negative charges, that is, the water molecules are oriented differently to the ion around the poles, forming a weakly bound hydrate sphere. When these dipole ions meet with appropriate orientation, the electrostatic attraction is still considerable between them thus a binuclear $(FeSO_4)_2^{2+}$ is easily formed as a transient species, which dissociates into Fe^{3+} and $Fe(SO_4)_2^-$. As $Fe(SO_4)_2^-$ is evidently much more weakly hydrated than SO_4^{2-}, the Fe^{3+} reacts much faster with the bisulfate complex than with the sulfate ion, that is, (R7) is fast in both directions. The formation of the well-known $(FeOH)_2^{4+}$ species in detectable concentration also supports the assumption of a similar species with two sulfates—instead of OH^- ions—acting as bridges between two metal ions. In the light of the considerations above, we tried to include $(FeSO_4)_2^{2+}$ into the equilibrium model also as the sixth light-absorbing species. (Note that the linear algebraic analysis detected only five absorbing species!) The agreement between the experimental and calculated data is improved in negligible extent. In other words, we do not have definite proof of its existence in considerable amount, that is, $(FeSO_4)_2^{2+}$ is best regarded as a kinetically important transient species.

Interpretation of the Shape of the Measured Curves. Taking into account the complex pattern of the change of concentrations (Fig. 6), the strict first-order shape of the curves—i.e., the seemingly simple possibility of describing the kinetics based on Fig. 3—needs some explanations. It is easy to realize that only a small amount of bisulfate complex is formed if the sulfate concentration is low. Since the pH is constant and $[SO_4^{2-}] \gg T_{Fe^{III}}$ in such samples, the shape of the expected absorbance vs. time series is first order and the pseudo-first-order rate constants are determined by (R3) and (R4) only. At higher sulfate concentrations, the bisulfate formation determines the absorbance change but it is formed through the fast (R7) and the rate-determining steps remain (R3) and (R4) resulting the first-order shape.

It is interesting to show the evaluation of our pseudo-first-order data based on Fig. 3, especially because most of the stopped-flow kinetic experiments are interpreted by using (pseudo-)first-order rate constants only. The nonzero intercept and the pH-dependent lines suggest two equilibrium processes:

$$Fe^{3+} + SO_4^{2-} \rightleftharpoons FeSO_4^+ \qquad \text{(R10)}$$

$$Fe(OH)^{2+} + SO_4^{2-} \rightleftharpoons FeSO_4^+ + OH^-. \qquad \text{(R11)}$$

If the correct approximations of $[SO_4^{2-}] \gg T_{Fe^{III}}$ and $[Fe(OH)^{2+}] \gg [Fe^{3+}]$ are applied, then the

$$k_{pseudo} = k_{-10} + k_{-11}\frac{K_w}{[H^+]} + \frac{k_{10} + k_{11}\frac{\beta_{1-10}}{[H^+]}}{1 + \beta_{011}[H^+]}T_{SO_4^{2-}}$$

equation could be derived from these two reactions. The rate constants calculated from this relation, however, are meaningless; $\log \beta_{101} = 1.4$ and 0.9 can be derived from the calculated k_{10}/k_{-10} and from the k_{11}/k_{-11} ratios, respectively, instead of about $\log \beta_{101} = 2.3$ determined by many authors [9–12] and in our present work. More interestingly, the parameter estimation with steps (R10) and (R11) gives an average deviation of 0.0036 AU, which is only slightly worse than the best fit with our suggested model (0.0028 AU). However, this result requires the fitting of the molar absorbances and the baselines, as well, and the fitted values are completely unacceptable (e.g., larger baseline than 0.1 AU). The individual pseudo-first-order fit, however, is not sensitive to these values.

This example convincingly shows that the (pseudo-) first-order interpretation of the stopped flow experiments may lead to absolutely incorrect results, even if all the conditions applied in the (pseudo-) first-order approximation are correct.

Evaluation

The advantages of the sophisticated evaluation methods developed by us recently [13–17] are the following:

Simultaneous Curve Fitting

- In the case of equilibrium measurements, it makes possible the precise photometric determination of an equilibrium constant between nonabsorbing species. It was shown that the change of $\log \beta_{011}$ by only 0.05 unit may lead to false identification of a species which otherwise is not formed in detectable concentration.
- The model-free MRA and $\mathcal{M}^3$ were ab ovo elaborated for simultaneous fitting. These programs set a limit on the number of independent absorbing species, above which any attempt to apply an equilibrium or kinetic model unavoidably runs into numerical difficulty or failure.
- In kinetics, the simultaneous evaluation makes possible to apply all the constraints (number

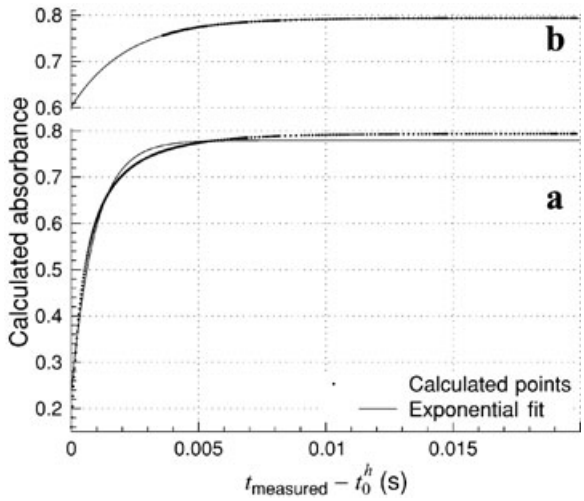

Figure 7 Exponential fit of the calculated absorbance–time series in case of sample 18. (a) The whole curve fitted from the hypothetical starting time. (b) The exponential fit of the measurable part of the curve.

of species, total concentrations, molar absorbances, formation constants) known from independent measurements. Therefore—even if only exponential kinetic curves can be measured—the second-order processes (R6, R7) may also be identified. This would be impossible by using the usual curve by curve apparent rate constants for evaluation. For illustration, Fig. 7 shows the calculated absorbance–time series in case of sample 18 at 304 nm. It is seen that the whole curve cannot be fitted with exponential function (Fig. 7a). If, however, only that part of the curve is fitted, which is actually measured by stopped flow, the exponential fit is practically perfect.

Filling Time and Starting Time vs. Dead Time. Simultaneous curve fitting alone is not suitable to extract experimental information precisely from stopped-flow signals. In case of fast reactions, the concentrations change significantly along the cuvette, thus the measured average signal may only be determined by integration through the time range necessary to fill the cuvette (t_f). It was mathematically proven in our previous work [17] that the dead time is not constant, it changes between $-t_0^h - \frac{1}{2}t_f$ and $-t_0^h - t_f$ depending on the pseudo-first-order rate constant. The evaluation method developed earlier can handle this not only for first order but any type of reactions. For the sake of comparison, all calculations were repeated by using a single dead time for all curves, instead of the starting and filling time. Table VI summarizes the average deviations. The σ values indicate that the differences

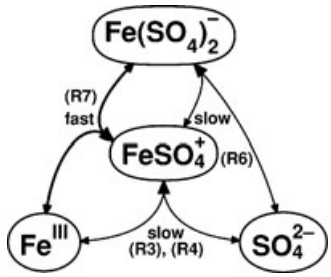

Figure 8 The skeleton of the kinetics for the formation of iron(III)–sulfate complexes. The equilibrium steps interpreted in Table V are in parenthesis.

between the calculations and the experiments are much higher than the experimental uncertainty, even for the best model when dead time was used. Moreover, omission of (R6) does not increase the deviation noticeably so the dead time concept may have led to false conclusion on the kinetics of the system.

SUMMARY

A comprehensive equilibrium and kinetic study of the iron(III)–sulfate system has been carried out using our recently elaborated evaluation methods. At higher sulfate concentrations ($[SO_4^{2-}] > 0.2$ M), the formation of bisulfate complex was detected and its stability constant was determined. Sophisticated evaluation of the kinetic experiments led to the conclusion that

$$2FeSO_4^+ \rightleftharpoons Fe(SO_4)_2^- + Fe^{3+}$$

has a decisive role in the bisulfate complex formation. The scheme of the proposed mechanism is given in Fig. 8. The advantages of the recently elaborated evaluation methods are briefly outlined.

SUPPLEMENTARY MATERIAL

The whole experimental data set is available in a supplementary file on the journal's homepage at http://www.interscience.wiley.com/jpages/0538-8066/suppmat/. Additional figures are also available to show the full series of the experimental curves and to detail or illustrate some steps of the evaluation. Although they are not necessary to understand the work and interpretations presented here, they can visualize some facts and they can make reading easier. These figures are referred as Figure Sx in this paper, where x is the number of the figure given in the supplementary file.

BIBLIOGRAPHY

1. Whiteker, R. A.; Davidson, N. J Am Chem Soc 1953, 75, 3081–3085.
2. Lister, M. W.; Rivington, D. E. Can J Chem 1955, 33, 1591–1602.
3. Nikolajeva, N. M.; Cvelodub, L. D. Z Neorg Khim 1975, 20, 3033–3037.
4. Davis, G. G.; Smith, W. M. Can J Chem 1962, 40, 1836.
5. Sapieszko, R. S.; Patel, R. C.; Matilevic, E. J Phys Chem 1977, 81, 1061–1068.
6. Khoe, G. H.; Rolins, R. G. J Chem Soc, Dalton Trans 1988, 2015–2021.
7. Stipp, S. L. Environ Sci Technol 1990, 24, 699–706.
8. Brown, P. L.; Sylva, R. W. J Chem Res (S) 1987, 4–5.
9. Feng, Q.; Waki, H. Polyhedron 1988, 7, 291–295.
10. Wendt, H.; Strehlow, H. Z Elektrochemie 1962, 66, 228–234.
11. Cavasino, F. P. J Phys Chem 1968, 72, 1378–1384.
12. Baker, F. L.; Smith, W. M. Can J Chem 1970, 48, 3100–3103.
13. Zékány, L.; Nagypál, I.; Peintler, G. PSEQUAD for Chemical Equilibria, Update 5.01, 2003. Available at http://www.staff.u-szeged.hu/˜peintler/enindex.htm
14. Peintler, G. ZiTa, A Comprehensive Program Package for Fitting Parameters of Chemical Reaction Mechanisms, Version 5.1, Department of Physical Chemistry, SzTE, Szeged, Hungary, 2001. Available at http://www.staff.u-szeged.hu/˜peintler/enindex.htm
15. Peintler, G.; Nagypál, I.; Jancsó, A.; Epstein, I. R.; Kustin, K. J Phys Chem A, 1997, 101, 8013–8020. Available at http://www.staff.u-szeged.hu/˜peintler/enindex.htm
16. Peintler, G.; Nagypál, I.; Epstein, I. R.; Kustin, K. J Phys Chem A, 2002, 106, 3899–3904. Available at http://www.staff.u-szeged.hu/˜peintler/enindex.htm
17. Peintler, G.; Nagy, A.; Horváth, A. K.; Körtvélyesi, T.; Nagypál, I. Phys Chem Chem Phys 2000, 2, 2575–2586.
18. Lente, G.; Fábián, I. Inorg Chem 1999, 38, 603–605.
19. Norris, A. C. Computational Chemistry; Wiley: New York, 1981; ch. 2, pp. 19–37.
20. Nagypál, I.; Beck, M. Chemistry of Complex Equilibria; Ellis-Horwood: Chichester, UK, 1990; ch. 4, p. 136.
21. IUPAC-Academic Software, Stability Constants Database Release 2, Otley, 1996.